Ionic Conductivity and Structural Phase Transformations for Hexagonal and Cubic $Bi_{1.33}U_{0.33}La_{0.33}O_{3.5}$ Polymorphs

J. M. Amarilla,* R. M. Rojas, and J. M. Rojo

Instituto de Ciencia de Materiales de Madrid, Consejo Superior de Investigaciones Cientificas, Cantoblanco, 28049 Madrid, Spain

Received December 6, 1996. Revised Manuscript Received March 5, 1997[⊗]

The hexagonal and cubic $Bi_{1.33}U_{0.33}La_{0.33}O_{3.5}$ polymorphs have been synthesized by heating at 950 °C a mixture of Bi_2O_3 and $LaUO_{4+x}$. When the reaction mixture is slowly cooled to room temperature, the hexagonal phase with cell parameters $a_H = 4.0285(3)$ Å, $c_H = 9.5494(8)$ Å is formed. Quenching of the mixture from 950 °C leads to the formation of the cubic phase with a fluorite-type structure, $a_C = 5.641(1)$ Å. The hexagonal and cubic materials are good oxide ion conductors, the conductivity being higher for the cubic polymorph. The conductivity vs temperature for both polymorphs shows several linear dependencies, which are ascribed to different crystalline phases identified by X-ray powder diffraction. An intermediate hexagonal phase different from the starting hexagonal one is found. The schemes of the structural transformations with temperature are established, and the relationships between conductivity properties and phase transformations are pointed out.

Introduction

Due to the excellent oxide-ion conductivity properties exhibited by the cubic δ-Bi_2O_3 phase, stabilization at room temperature of this high-temperature polymorph has been attempted by doping with several oxides, mainly Ln_2O_3 (Ln = lanthanide including Y)[1−4] and MO (M = Ca, Sr, Ba).[5−7] Solid solutions formed in the Bi_2O_3−M_2O_3 (M = Ln, Y) and Bi_2O_3−MO (M = Ca, Sr, Ba) systems show on average, cubic or rhombohedral structures, respectively.[8−12] Oxides of high-charge cations such as M_2O_5 (V, Nb, Ta) have also been used as dopants.[13] In the case of V_2O_5, it has given way to the so-called BIMEVOX family, derived from $Bi_4V_2O_{11}$,[14−18] in which vanadium and/or bismuth are partly substituted by iso- or aliovalent cations. In the $(Bi_2O_3)_{1-x}$-$(WO_3)_x$ system a cubic phase has also been stabilized.[19,20] However, it has been shown that in general, the stabilized cubic δ phases are quenched high-temperature metastable phases which, on annealing, transform into the stable low-temperature modification.[21−27] This is a severe limitation for the long-term stability requirements for potential technological applications of these materials as solid electrolytes in electrochemical devices. In some cases, the addition of two dopants seems to improve the stabilization of the face-centered cubic (fcc) structure, while maintaining a high conductivity.[28−30] In other cases, addition of aliovalent cations can suppress structural transformations which would otherwise occur on aging.[31,32]

In a previous paper[33] we reported on the synthesis of $Bi_{1.33}U_{0.33}La_{0.33}O_{3.5}$, which constitutes the member at $x = 0.333$ of the new bismuth-based oxide materials of general formula $Bi_{2-2x}U_xLa_xO_{3+3x/2}$ ($0.333 \le x \le 0.038$). It was synthesized from a mixed ceramic/organic pre-

* To whom correspondence would be addressed.

[⊗] Abstract published in *Advance ACS Abstracts,* April 15, 1997.

(1) Takahashi, T.; Iwahara, H.; Nagai, Y. *J. Appl. Electrochem.* **1972**, *2*, 97.
(2) Takahashi, T.; Iwahara, H. *Mater. Res. Bull.* **1978**, *13*, 1447.
(3) Verkerk, M. J.; Keizer, K.; Burggaarf, A. J. *J. Appl. Electrochem.* **1980**, *10*, 81.
(4) Verkerk, M. J.; Burggaarf, A. J. *J. Electrochem. Soc.* **1981**, *128*, 75.
(5) Conflant, P.; Boivin, J. C.; Tridot, T. *C. R. Acad. Sci. Paris, Ser. C* **1974**, 457.
(6) Conflant, P.; Boivin, J. C.; Thomas, D. *J. Solid State Chem.* **1976**, *18*, 133.
(7) Guillermo, R.; Conflant, P.; Boivin, J. C.; Thomas, D. *Rev. Chim. Miner.* **1978**, *15*, 153.
(8) Iwahara, H.; Esaka, T.; Sato, T.; Takahasi, T. *J. Solid State Chem.* **1981**, *39*, 173.
(9) Conflant, P.; Boivin, J. C.; Thomas, D. *J. Solid State Chem.* **1980**, *35*, 192.
(10) Boivin, J. C.; Thomas, D. *Solid State Ionics* **1981**, *5*, 523.
(11) Tilley, R. J. D. *J. Solid State Chem.* **1982**, *41*, 233.
(12) Withers, R. L.; Rossell, H. *J. Solid State Chem.* **1995**, *118*, 66.
(13) Takahashi, T.; Iwahara, H.; Esaka, T. *J. Electrochem. Soc.* **1977**, *124*, 1563.
(14) Abraham, F.; Debreville-Gresse, M. F.; Mairesse, G.; Nowogroki, G. *Solid State Ionics* **1988**, *28−30*, 529.
(15) Vannier, R. N.; Mairesse, G.; Abraham, F.; Nowogroki, G. *Solid State Ionics* **1994**, *70−71*, 248.
(16) Joubert, O.; Jouanneaux, A.; Ganne, M.; Vannier, R. N.; Mairesse, G. *Solid State Ionics* **1994**, *73*, 309.
(17) Lee, Ch. K.; Lim, G. S.; West, A. R. *J. Mater. Chem.* **1994**, *4*, 1441.
(18) Yan, J.; Greenblatt, M. *Solid State Ionics* **1995**, *81*, 225.
(19) Takahashi, T; Iwahara, H. *J. Appl. Electrochem.* **1973**, *3*, 65.
(20) Zhou, W. *J. Solid State Chem.* **1994**, *108*, 381.
(21) Watanabe, A.; Kikuchi, T. *Solid State Ionics* **1986**, *21*, 287.
(22) Watanabe, A. *Solid State Ionics* **1990**, *40/41*, 889.
(23) Watanabe, A.; Drache, M.; Wignacourt, J. P.; Conflant, P.; Boivin, J. C. *Solid State Ionics* **1993**, *67*, 25.
(24) Jiang, N.; Buchanam, R. M.; Fenn, F. E. G.; Marshall, A. F.; Stevenson, D. A.; Wachsman, E. D. *Mater. Res. Bull.* **1994**, *29*, 247.
(25) Jiang, N.; Buchanam, R. M.; Stevenson, D. A.; Nix, W. D.; Li, J. Z.; Yang, J. L. *Mater. Lett.* **1995**, *22*, 215.
(26) Watanabe, A. *Solid State Ionics* **1995**, *79*, 84.
(27) Watanabe, A. *J. Solid State Chem.* **1995**, *120*, 32.
(28) Meng, G.; Chen, Ch.; Han, X.; Yang, P.; Peng, P. *Solid State Ionics* **1988**, *28−30*, 533.
(29) Hu, K.; Chen, Ch.; Peng, D.; Meng, G. *Solid State Ionics* **1988**, *28−30*, 566.
(30) Mercurio, D.; El Farissi, M.; Frit, B.; Reau, J. M.; Senegas, J. *Solid State Ionics* **1990**, *39*, 297.
(31) Fung, K. Z.; Baek, H. D.; Virkar, A. V. *Solid State Ionics* **1992**, *52*, 199.
(32) Fung, K. Z.; Cheng, J.; Virkar, A. V. *J. Am. Ceram. Soc.* **1993**, *76*, 2403.
(33) Amarilla, J. M.; Rojas, R. M.; Herrero, M. P. *Chem. Mater.* **1995**, *7*, 341.

S0897-4756(96)00624-2 CCC: $14.00

cursor and at room temperature has hexagonal symmetry, space group $P\bar{3}$, $a_H = 3.9937(8)$ Å, $c_H = 9.728(2)$ Å. It was shown[34] that unlike other compositions, the hexagonal polymorph does not transform even after a long annealing period (600 °C for 500 h), indicating a very high stability on aging. The hexagonal phase transforms at ≈850 °C into a cubic fluorite-type phase (space group $Fm3m$, $a_C = 5.6378(1)$ Å). Preliminary conductivity measurements carried out on both the hexagonal and the quenched cubic $Bi_{1.33}U_{0.33}La_{0.33}O_{3.5}$ polymorphs in the temperature range 300−550 °C showed that these materials could be included among the best oxide ion conductors. The aim of this paper is to study in detail the oxide ion conductivity of the hexagonal and cubic $Bi_{1.33}U_{0.33}La_{0.33}O_{3.5}$ polymorphs. Changes in conductivity are discussed in terms of temperature-dependent structural transformations.

Experimental Section

Both hexagonal (H) and cubic (C) $Bi_{1.33}U_{0.33}La_{0.33}O_{3.5}$ oxides were synthesized by thorough mixing of stoichiometric amounts of α-Bi_2O_3 and lanthanum uranate $LaUO_{4+x}$, which was previously obtained from thermal decomposition at 850 °C of the organic precursor lanthanum uranyl propionate $LaUO_2(C_2H_5COO)_5 \cdot 3H_2O$. The mixture was heated in air at 2 °C min^{-1} to 950 °C and kept at this temperature for 24 h. Then it was cooled at 2 °C h^{-1} to 600 °C and then cooled again at 2 °C min^{-1} to room temperature. This procedure, which is an alternative to the mixed ceramic/organic precursor method, yielded a very well crystallized microcrystalline material with hexagonal cell parameters, $a_H = 4.0285(3)$ Å, $c_H = 9.5494(8)$ Å. The cubic $Bi_{1.33}U_{0.33}La_{0.33}O_{3.5}$ phase was synthesized following the same procedure, but after the heating treatment at 950 °C the sample was quenched in air.

X-ray powder diffraction patterns were recorded at room temperature with a Siemens D-501 diffractometer, with Cu Kα radiation. X-ray patterns have been scanned at 0.02° (2θ) and 5 s/step counting time within the range $4 \leq 2\theta \leq 120°$. Cell parameters have been refined by using the program CELREF.[35] Differential thermal analysis (DTA) and thermogravimetric (TG) curves have been simultaneously recorded on a Stanton STA 781 instrument. A ≈80−100 mg batch of each sample has been heated in air at 10 °C min^{-1}; α-Al_2O_3 has been used as reference material. Moreover, ≈80−100 mg batches of the hexagonal and cubic samples have been kept in the DTA equipment at some specific temperatures for 10 min and then quenched to room temperature by rapidly removing them from the furnace. Differential scanning calorimetry (DSC) measurements have been performed in a Seiko DSC 320U instrument at a 10 °C min^{-1} heating/cooling rate. Electrical conductivity measurements have been carried out by the complex impedance method using a Solartron 1174 frequency response analyzer connected to a Solartron 1286 electrochemical interface. Pellets of ≈6 mm diameter and 1 mm thickness were prepared by compacting the powder sample under a pressure of 1500 kg m^{-2}. Pellets of the hexagonal phase were sintered at 950 °C for 12 h and then cooled at 1 °C min^{-1} to room temperature while those of the cubic phase were quenched in air from 950 °C. Platinum electrodes were painted on the two planar surfaces of the sintered pellets with platinum paste (Engelhard 6082); then they were dried at 200 °C for 1 h and fired at 950 °C for 4 h. The pellet of the hexagonal phase was slowly cooled from 950 °C to room temperature (1 °C min^{-1}), and the pellet corresponding to the cubic phase was quenched in air. Before the electrical measurements the crystalline phase of each pellet was checked by X-ray powder diffraction. The impedance measurements were carried out in the frequency range $1-10^5$ Hz at different temperatures (190−980 °C) with the pellet in still air. In the heating and cooling runs the increment of temperature was 30 °C, and before each measurement the sample was kept at the indicated temperature for 20 min.

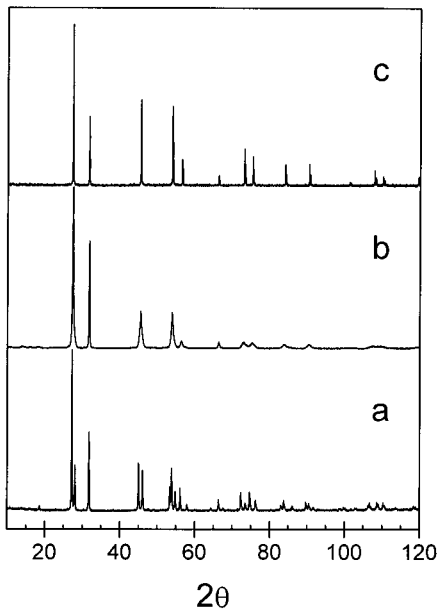

Figure 1. X-ray diffraction patterns recorded at room temperature for $Bi_{1.33}U_{0.33}La_{0.33}O_{3.5}$ synthesized: (a) by the ceramic procedure used in this work; b) by a mixed organic precursor/ceramic procedure used in ref 33; (c) either (a) or (b) quenched from 950 °C.

Results

X-ray Powder Diffraction. The X-ray powder diffraction pattern of the room-temperature hexagonal $Bi_{1.33}U_{0.33}La_{0.33}O_{3.5}$ polymorph prepared by the ceramic procedure used in this work is presented in Figure 1a; its powder diffraction data are summarized in Table 1. It crystallizes in the hexagonal system with cell parameters $a_H = 4.0285(3)$, $c_H = 9.5494(8)$ Å, ($c_H/a_H = 2.37$), and $V_H = 134.21$ Å^3. In Figure 1b the X-ray pattern of the material synthesized by the mixed ceramic/organic precursor procedure previously described[33] is shown for comparison. The cell constants for this latter material are $a_H = 3.9937(8)$ Å, $c_H = 9.728(2)$ Å ($c_H/a_H = 2.43$). Annealing of both hexagonal polymorphs at 600 °C for 500 h does not modify the material, and the X-ray patterns remain identical with those shown in Figure 1a,b. When any of the hexagonal phases are heated from room temperature to 950 °C and then quenched in air, a face-centered cubic fluorite-type phase (Figure 1c) is isolated. The lattice constant for the cubic phase synthesized from the hexagonal polymorph prepared by the ceramic procedure is $a_C = 5.641(1)$ Å ($V_C = 179.50$ Å^3).

Thermal Behavior. The thermogravimetric curve recorded up to 950 °C (not shown) indicates that neither the hexagonal or cubic polymorph experiences any significant weight variation with temperature. Figure 2 shows the calorimetric curve obtained for the hexagonal phase from room temperature to 950 °C at 10 °C min^{-1} heating/cooling rate. In the heating process a small endothermic effect at 500−540 °C, and an asymmetric peak with onset and minimum temperatures 838 and 858 °C, respectively, are observed. Enlarged areas of these zones are shown in the insets of Figure 2. The

(34) Amarilla, J.M.; Rojas, R. M. *Chem. Mater.* **1996**, *8*, 401.
(35) Laugier, J.; Filhol, A. (CELREF), I. L. L. Grenoble, France, unpublished, P.C. version, 1991.

Table 1. X-ray Powder Diffraction Pattern of Hexagonal $Bi_{1.33}U_{0.33}La_{0.33}O_{3.5}$ Synthesized by the Ceramic Procedure Used in This Work[a]

h k l	$2\theta_{exp}$	$2\theta_{cal}$	*d* (Å)	I/I_0
0 0 2	18.538	18.568	4.786	2
0 1 1	27.184	27.192	3.280	100
0 0 3	27.988	28.008	3.188	28
0 1 2	31.734	31.740	2.820	54
1 0 3	38.270	38.244	2.352	1
1 1 0	44.974	44.968	2.0156	33
1 0 4	46.028	46.030	1.9718	27
0 0 5	47.564	47.572	1.9117	1
1 1 2	49.036	49.046	1.8577	1
2 0 1	53.360	53.346	1.7169	17
1 1 3	53.826	53.816	1.7031	31
0 1 5	54.748	54.750	1.6766	13
2 0 2	56.086	56.086	1.6397	18
0 0 6	57.898	57.892	1.5927	1
1 0 6	64.286	64.278	1.4490	2
2 0 4	66.314	66.310	1.4095	8
1 1 5	67.510	67.532	1.3874	2
1 2 1	72.268	72.272	1.3073	13
0 2 5	73.470	73.462	1.2889	5
2 1 2	74.632	74.606	1.2717	13
1 1 6	76.180	76.172	1.2496	7
3 0 0	82.990	82.964	1.1635	3
2 1 4	83.730	83.726	1.1551	7
0 1 8	86.014	86.008	1.1302	3
3 0 3	89.682	89.692	1.0932	6
1 2 5	90.440	90.450	1.0860	5
0 2 7	91.600	91.586	1.0753	2
2 1 6	98.702	98.684	1.0161	1
2 2 0	99.798	99.788	1.0078	2
0 2 8	102.866	102.878	0.9860	1
3 1 1	106.254	106.290	0.9637	3
2 2 3	106.656	106.686	0.9611	5
3 1 2	108.660	108.636	0.9489	5
3 0 6	110.264	110.242	0.9396	5
1 0 10	113.506	113.508	0.9218	2
3 1 4	118.378	118.406	0.8976	3
3 0 7	120.992	121.008	0.8858	3

[a] $a_H = 4.0285(3)$ Å, $c_H = 9.5494(8)$ Å, $c_H/a_H = 2.37$, $V_H = 134.21$ Å^3.

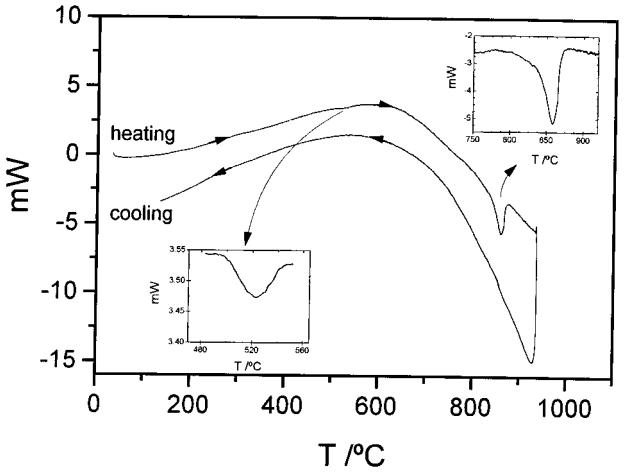

Figure 2. DSC curve recorded for hexagonal $Bi_{1.33}U_{0.33}La_{0.33}O_{3.5}$ at 10 °C min^{-1} heating/cooling rate. Thermal effects are enlarged and shown in the insets.

enthalpies of the reactions, deduced from the peak areas, are 0.12 and 5.06 J g^{-1} (0.027 and 1.16 kJ mol^{-1}), respectively. The DSC trace does not show any significant transformation on cooling. In Figure 3 the DSC trace recorded for the cubic fluorite-type material is presented. In this case, two consecutive exo- and endothermic effects are observed in the temperature range 730−880 °C, with enthalpies of 0.99 and 2.411 J g^{-1} (0.23 and 0.55 kJ mol^{-1}), respectively. Again, the

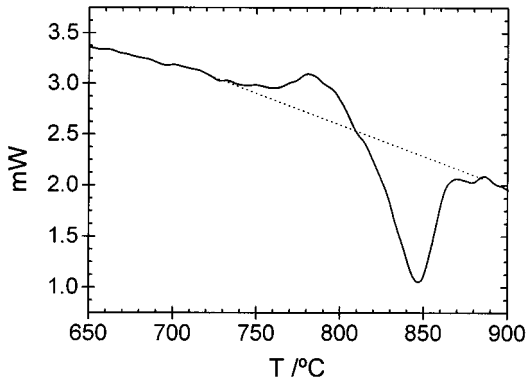

Figure 3. DSC heating curve recorded for $Bi_{1.33}U_{0.33}La_{0.33}O_{3.5}$ at 10 °C min^{-1}. Only the temperature range where transformations occur is presented.

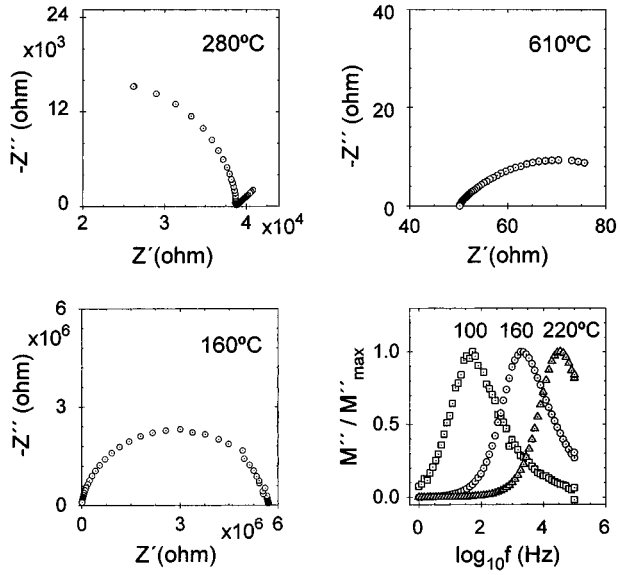

Figure 4. Impedance plots (imaginary vs real part) obtained at the indicated temperatures. Frequency (log *f*) dependence of the imaginary part of the normalized modulus (M''/M''_{max}) at 100, 160, and 220 °C is also included.

DSC curve does not show any noticeable thermal effect on cooling.

Electrical Measurements. The impedance plots $-Z''$ vs Z' of the hexagonal phase at different temperatures are shown in Figure 4. At low temperature (160 °C) an arc is observed. The capacitance associated with this arc is 20 pF, which is the order of magnitude usually reported for grain interior response.[36] When the pellet is heated at higher temperature (280 and 610 °C), the arc disappears progressively and a new arc is developed. This arc, which shows a capacitance of 30 mF, is ascribed to electrode reactions.[36] The frequency dependence (log *f*) of the imaginary part of the electrical modulus normalized with respect to its maximum value (M''/M''_{max}) is also shown in Figure 4. An asymmetric peak is observed. This peak shifts toward higher frequency when the sample is heated at increasing temperature.

Discussion

The impedance plot of a ceramic material may show two arcs due to the grain interior and grain boundary

(36) Bonanos, N.; Steele, B. C. H.; Butler, E. P. In *Impedance Spectroscopy*; Macdonald, J. R., Ed.; John Wiley: New York, 1987; p 191.

Table 2. Activation Energy (E), Preexponential Factor (log σ_0), and Conductivity (σ) Associated with Phases Detected at the Temperatures Indicated during the Thermal Treatments of the Hexagonal and Cubic $Bi_{1.33}U_{0.33}La_{0.33}O_{3.5}$ Material

run	T_{range} (°C)	X-ray phase[a]	E (eV)	log σ_0	temp (°C)	σ (Ω^{-1} cm^{-1})
		Hexagonal Phase				
heating and cooling	190−550	H	0.84	2.54	310	2.1×10^{-5}
						1.9×10^{-5}
heating and cooling	580−820	H*	1.10	4.06	700	2.3×10^{-2}
						2.6×10^{-2}
heating and cooling	880−970	C	0.86	2.56	910	2.6×10^{-1}
						2.7×10^{-1}
		Cubic Phase				
heating	190−340	C	0.85	3.19	310	8.3×10^{-5}
heating	370−580	C			460	1.4×10^{-3}
heating	610−820	H*	1.03	4.01	700	2.8×10^{-2}
heating and cooling	880−970	C	0.85	3.19	970	4.1×10^{-1}
cooling	760−580	H*	1.07	4.03	700	3.0×10^{-2}
cooling	550−190	H	0.85	2.73	310	2.5×10^{-5}

[a] C = face-centered cubic, H and H* = hexagonal.

responses. However, only one arc frequently occurs, which can bear information of either both responses or only the grain interior response, depending on the previous sintering treatment of the pellet.[37,38] Moreover, it is known that the electrical modulus gives information about the grain interior response and is not usually affected by grain boundary and electrode effects.[39] To determine whether the impedance arc observed at low temperature (below 300 °C) is affected by the grain boundary response, the activation energies deduced from modulus (M'') and conductivity (σ) data have been compared. The frequency corresponding to the maxima of the M'' peaks measured at different temperatures (Figure 4) was plotted as log f vs 1000/T. The experimental data (not shown) followed a linear dependence which was fitted to the expression $f = f_0 \exp(-E/k_BT)$, where f_0 is a preexponential factor, E the activation energy, k_B the Boltzmann constant, and T the temperature. An E value of 0.86 ± 0.02 eV was obtained; this value coincides within the experimental error with the value deduced from the conductivity plot log σ vs 1000/T (see Table 2). This fact indicates that the impedance arc observed at low temperatures is dominated by the grain interior response.

The resistance of the pellet at each temperature was determined by intersection of the impedance arc with the real axis, then the conductivity values were deduced as usual. Figure 5 shows the variation of the conductivity (log σ) vs inverse temperature (1000/T) for the hexagonal and cubic $Bi_{1.33}U_{0.33}La_{0.33}O_{3.5}$. For the hexagonal phase three regions that coincide for the heating and cooling treatments are observed. They range between 190 and 550, 580 and 820, and 880 and 970 °C. The experimental points for each region are well fitted by an Arrhenius equation, $\sigma = \sigma_0 \exp(-E/k_BT)$, where σ_0, E, k_B, and T have the usual meaning.

To investigate the origin of the three conductivity regions, a ≈100 mg batch of the hexagonal sample was cumulatively heated to some specific temperatures between 600 and 900 °C, kept at each temperature for 10 min, and then quenched in air by rapidly removing the sample from the furnace. The effectiveness of the quenching process has been confirmed by an experiment carried out on a high-temperature X-ray diffraction chamber.

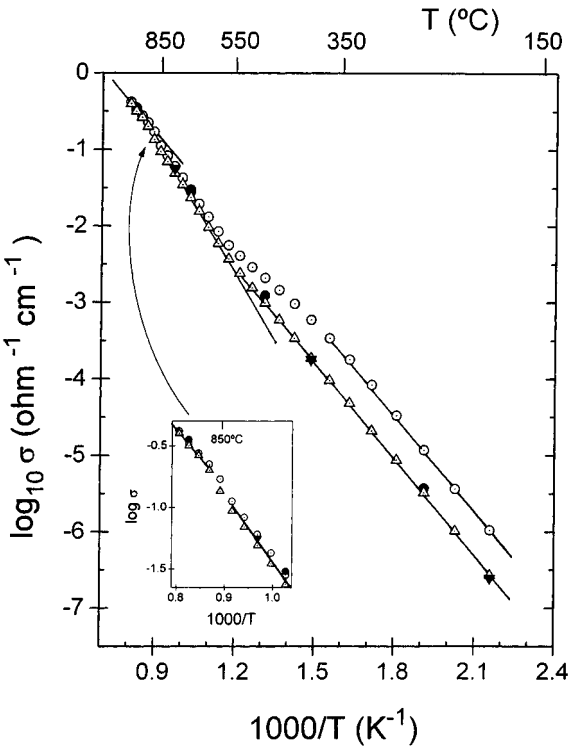

Figure 5. Plot of log σ vs 1000/T for both hexagonal and cubic $Bi_{1.33}U_{0.33}La_{0.33}O_{3.5}$ polymorphs. The symbols Δ and ○ stand for the hexagonal and cubic phases. Open and closed symbols refer to the heating and cooling runs, respectively.

The X-ray pattern of the sample at 600 °C (Figure 6a, dotted line) is the same as that of the starting hexagonal phase (Figure 1a). Therefore the Arrhenius dependence observed in the range 190−550 °C is ascribed to the hexagonal phase. When the sample is quenched from 750 °C (Figure 6a, solid line) the X-ray pattern can be fully indexed on the basis of another hexagonal cell (H*) with parameters very close to those determined for the initial hexagonal (H) phase (Figure 6a, dotted line). The c parameter has slightly increased (+0.15%) for the H* cell showing a value of 9.564(1) Å. The a parameter for the H* cell (a_{H^*} = 4.0247(5) Å) has decreased (−0.09%) as compared with that parameter of the H cell. The opposite variation of the lattice

(37) Bonanos, N,; Drennan, J.; Slowinski, R. K.; Steele, B. C. H.; Butler, E. P. *Silicates Ind.* **1985**, *9−10*, 127.
(38) Martínez-Juárez, A.; Iglesias, J. E.; Rojo, J. M. *Solid State Ionics* **1996**, *91*, 295.
(39) Hodge, I. M.; Ingram, M. D.; West, A. R. *J. Electroanal. Chem.* **1976**, *74*, 125.

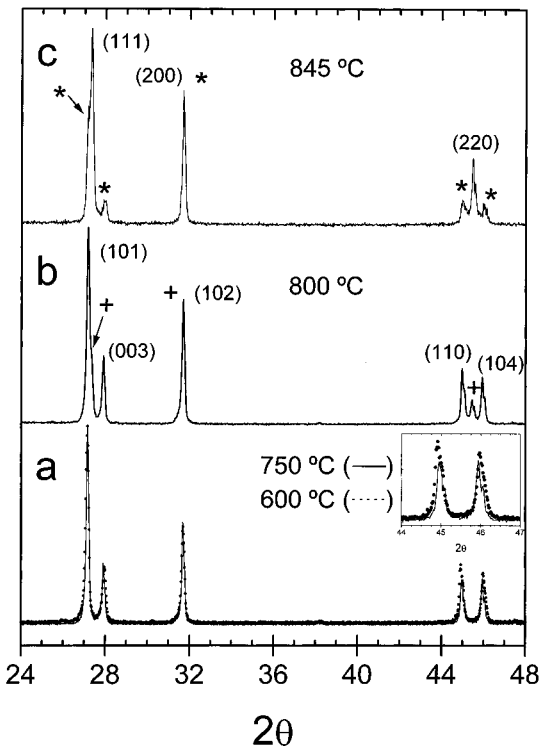

Figure 6. X-ray patterns recorded for hexagonal $Bi_{1.33}U_{0.33}La_{0.33}O_{3.5}$ quenched from (a) 600 °C (···); 750 °C (—); (b) 800 °C; maxima of the cubic phase are marked +; (c) 845 °C; maxima of the hexagonal phase are marked *. (The pattern at 600 °C (···) is identical with that of the starting hexagonal phase shown in Figure 1a.)

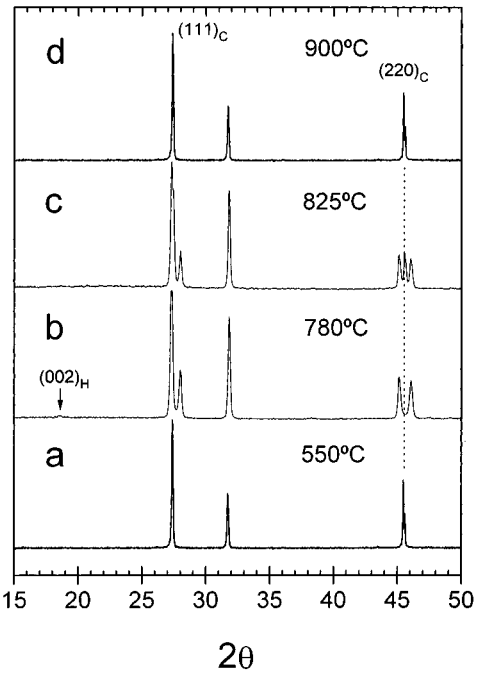

Figure 7. X-ray patterns recorded for cubic $Bi_{1.33}U_{0.33}La_{0.33}O_{3.5}$ quenched from the temperatures indicated.

constants for the H* phase indicates that the subtle H → H* transformation is not a pure dilatation. This transformation accounts for the change of slope observed in the Arrhenius plot between 550 and 580 °C (Figure 5) and for the small endothermic peak observed in the DSC curve of the hexagonal phase at $T_{max} = 523$ °C (see lower left inset in Figure 2). Moreover the presence of a new H* phase agrees with the second linear dependence observed between 580 and 820 °C (Figure 5). Between 820 and 880 °C, a small jump of conductivity is observed (see inset Figure 5), and above 880 °C the experimental data follow another linear dependence with different slope. The X-ray pattern recorded for the hexagonal sample quenched from 800 °C is shown in Figure 6b. In this pattern the $(220)_C$ diffraction peak of the cubic phase, centered at $2\theta \approx 45.4°$, is observed. Between this latter temperature and 845 °C the $(111)_C$ and $(220)_C$ peaks (marked + in Figure 6b) have progressively developed, while the intensity of $(110)_H$ and $(104)_H$ maxima (marked * in Figure 6c) have significantly decreased. At 900 °C the pattern is identical with that shown in Figure 1c, indicating that at this temperature the material is obtained as a cubic single phase. These results show that the H* → C transformation takes place in the temperature interval 800−870 °C, and it accounts for the small jump of conductivity between 820 and 880 °C (see inset in Figure 5) and for the asymmetric endothermic DSC effect centered at 858 °C (see upper right inset in Figure 2). Then, the third linear dependence observed for conductivity in Figure 5 is ascribed to the cubic fluorite-type polymorph. For the cooling treatment, the conductivity values (closed triangles in Figure 5) are practically the same as for the heating run. This fact, together with X-ray patterns recorded on cooling, show that the structural H → H* → C transformations are reversible with temperature.

The conductivity values for the cubic $Bi_{1.33}U_{0.33}La_{0.33}O_{3.5}$ phase are represented in Figure 5 as open and closed circles for the heating and cooling runs, respectively. For the heating run, between 190 and 340 °C a straight line fits well the experimental points. This line also fits the conductivity data obtained in the highest temperature interval (880−970 °C), in agreement with the fact that at high temperature we are dealing with the same cubic phase existing at low temperature. Between 370 and 580 °C, the experimental data depart from the Arrhenius behavior shown by the low-temperature cubic phase, and above 580 °C the conductivity follows the same dependencies observed for the H* and C phases in the ranges 610−820 and 880−970 °C, respectively. Although the Arrhenius behavior characteristic of the C phase is not followed between 370 and 580 °C, no change in the symmetry of the starting C phase was detected by X-ray diffraction (Figure 7a). However, the conductivity data suggest a change in the movement of O^{2-} ions in a large temperature range before the C → H* transformation. The X-ray patterns recorded for the cubic sample quenched from 780 (Figure 7b) and 900 °C (Figure 7d) confirm the formation of the hexagonal H* and cubic C as single phases in the temperature ranges already mentioned, and allow us to ascribe the small exo- and the endothermic effects observed in the DSC curve (Figure 3) to the C → H* and H* → C transformations, respectively. As in the case of the hexagonal polymorph, the latter H* → C transformation also takes place between 800 and 900 °C (Figure 7c). In the cooling treatment the cubic sample behaves differently from heating. In fact, the conductivity data (closed circles in Figure 5) are very close to those obtained for the hexagonal polymorph, showing the three linear dependencies already described; i.e., on cooling the C phase is transformed to the intermediate H* phase and finally into the hexagonal H phase. It is worth mentioning that when the

cubic phase is slowly cooled from temperatures below 580 °C, X-ray diffraction data show that the cubic phase is maintained. However, when it is slowly cooled from temperatures above the C → H* transition, the hexagonal H polymorph is formed. A long annealing process carried out on this latter H polymorph shows that this hexagonal phase is very stable on aging. This is a remarkable result for potential technological applications.

From the slope of the straight lines in Figure 5, the activation energy (E) associated with motion of O^{2-} has been determined. The temperature ranges in which the phases are detected, the activation energy (E), preexponential factor ($\log \sigma_0$) and conductivity (σ) associated with those phases are outlined in Table 2. It is observed that E shows the same value within the experimental error (0.85 ± 0.02 eV) for the H and C phases. Therefore, the better conductivity observed for the C phase is due to a higher preexponential factor. In contrast, the E value for the intermediate H* phase is higher than that for the H and C phases. Conductivities shown by the H, H*, and C phases (see Table 2) are within the range of those reported for the best oxide ions conductors such as rhombohedral $(Bi_2O_3)_{0.8}(SrO)_{0.2}$ (2.7×10^{-1} $\Omega^{-1}\cdot cm^{-1}$) or cubic $(Bi_2O_3)_{0.75}(Y_2O_3)_{0.25}$ (3.5×10^{-1} $\Omega^{-1} \times cm^{-1}$) at 800 °C[40,41] and are, at least 1 order of magnitude higher than those of yttria stabilized zirconia (YSZ) at the same temperatures.

Acknowledgment. Financial support by CICyT (Project MAT95/0899) is gratefully acknowledged.

CM960624X

(40) Takahashi, T. In *Superionic Solids and Solid Electrolytes*; Laskar, A. L., Chandra, S., Eds.; Academic Press Inc.: San Diego, 1989; p 1.

(41) Azad, A. M.; Larose, S.; Akbar, S. A. *J. Mater. Sci.* **1994**, *29*, 4135.